Energy Advances

ROYAL SOCIETY OF CHEMISTRY

PAPER

View Article Online
View Journal

Cite this: DOI: 10.1039/d6ya00042h

Aqueous polypyrrole : carboxymethyl cellulose conducting binder for graphite electrodes in lithium-ion batteries

Anh Ngoc Tram Mai and Christian Kuss *

In lithium-ion batteries (LIBs), polymeric binders are utilized to ensure the mechanical integrity of composite electrodes and facilitate ion transport. Compared to conventional fluoropolymers, such as polyvinylidene fluoride (PVDF), water-processable polymers are advantageous from both ecological and economic standpoints. Aqueous sodium carboxymethyl cellulose (CMC-Na) and its composites with elastomers have been established as fluorine-free alternatives to conventional fluorinated binders in lithium intercalation anodes. Unlike the low polarity PVDF, CMC possesses functional groups (–COOH and –OH) that can strengthen interactions with other materials through hydrogen bonding and covalent bonding. CMC is also cost-effective, water-soluble, and biodegradable. To create a multifunctional binder with CMC and eliminate the need for conductive additives, our group previously synthesized conductive CMC composites by using CMC as a dopant in polypyrrole (PPy). As a conducting polymer in its oxidized form, it provides good conductivity and thermal and environmental stability. In this study, we report, for the first time, the application of PPy : CMC as a conducting binder in graphite anodes. Cycling stability, rate capability, and interfacial/charge transfer resistance were evaluated with galvanostatic cycling, cyclic voltammetry, and impedance spectroscopy, respectively. Degradation mechanisms and by-products were studied, and electrode morphology and homogeneity were characterized. It was found that although PPy : CMC is partially reduced under anode operating conditions, this does not adversely affect long-term battery cyclability. These findings establish PPy : CMC as a viable multifunctional binder for graphite anodes and provide new insight into the binder's behavior, laying the groundwork for its application in next-generation high-energy-density LIBs.

Received 20th February 2026,
Accepted 17th April 2026

DOI: 10.1039/d6ya00042h

rsc.li/energy-advances

Introduction

Lithium-ion batteries (LIBs) have become a preferred technology for powering electronic devices, hybrid and electric vehicles, and short- to mid-term stationary energy storage, aiding the transition from fossil fuels to renewable energy systems.[1] To optimize LIBs for these diverse applications, it is essential to develop materials that offer high electrochemical performance while being safe, cost-effective, sustainable, and scalable for next-generation high-power batteries. Although binders account for only small portions (2–5 wt%) in commercial electrodes and are often considered of minor significance, binders can significantly influence the electrochemical performance of energy-storage devices.[2] Binders are critical for (i) maintaining the electrode's mechanical and electronic integrity by bridging dispersed electrode particles together with a current collector *via* physical and chemical forces, (ii) promoting ion transport by facilitating electrolyte uptake and improving electrode wettability, and (iii) aiding in electrode fabrication.

Binder systems, which conventionally consist of fluorinated binders, *e.g.*, poly(vinylidene difluoride) (PVDF), and carbon conductive additives, provide adhesion and electronic conductivity. PVDF has been widely used in commercialized batteries due to its electrochemical, thermal, and environmental stability. However, PVDF is expensive, has limited binding strength, poor flexibility, and, upon release into the environment, contributes to persistent, bioaccumulative microplastic and PFAS contamination.[3] Electrode preparation with PVDF generally requires dissolution in the hazardous, flammable, expensive, and high-boiling solvent *N*-methyl-2-pyrrolidone (NMP), which increases overall cost and safety concerns during electrode processing (*i.e.* slurry mixing, electrode coating, drying) and solvent recovery. Moreover, traditional binders are proving inadequate for emerging high-capacity active materials, which require binders with improved mechanical properties and additional functionalities.[4,5] PVDF can also exhibit swelling issues in the presence of electrolytes, compromising its

University of Manitoba, Department of Chemistry, 144 Dysart Road, Winnipeg, Manitoba, R3T 2N2, Canada. E-mail: christian.kuss@umanitoba.ca

mechanical benefits.[6] These issues underscore the need to address the reliance on non-renewable chemicals and the environmental and safety risks associated with toxic manufacturing/disposal processes. To ensure the sustainability of future energy storage systems, it is crucial to develop greener binder systems with enhanced functionalities and environmental compatibility.

One approach to addressing the above issues is using biopolymer binders that are water-processable and biodegradable.[6,7] They commonly contain multiple functional groups that make them water-soluble as well as reinforce binding strength and improve mechanical and electrochemical performance. The most widely used bio-derived binder, carboxylmethyl cellulose (CMC), is significantly cheaper than PVDF and is commercially used in LIB graphite anodes. Interestingly, using CMC as a dopant in polypyrrole (PPy) yields PPy : CMC conductive polymers with tunable electrical and mechanical properties.[8] The composites have been investigated and applied in various fields, including conductive binders in $LiCoO_2$ cathode,[9] electrode materials in supercapacitors,[10] anode materials in microbial fuel cells,[11] or as adsorbents in wastewater treatment.[12] This is attributed to the PPy's high conductivity, redox activity, and facile production process.[13] However, the electrochemical behavior and degradation mechanisms of PPy : CMC as an alternative conductive binder in LIBs have not been well understood. In addition, as a p-type conductive polymer, PPy : CMC may undergo reduction or partial carbonization when used in lithium intercalation anodes. While the decomposition products resulting from partial carbonization can lead to increased irreversible capacity in the first cycle, they can contribute to the power density due to increased electronic conductivity and consequently improved power performance in subsequent cycles.[14,15] To the best of our knowledge, in this work, the applicability and effects of PPy : CMC in graphite anode, the dominant anode material in commercial LIBs, are studied for the first time. The study provides insights into the design and optimization of multifunctional binders for next-generation batteries, and a broad range of related and unconventional applications, *e.g.* charge storage devices, flexible electronics, sensors effluent treatment technology, *etc.*, that can be expected in the future.

Experimental

Materials and methods

Synthetic Graphite powder (20 microns), pyrrole (98%), sodium carboxymethyl cellulose (Na-CMC) (M_W = 250 000 Da, degree of substitution = 0.9), (Poly(vinylidene fluoride) (PVDF, average M_w ~534 000), *N*-methyl-2-pyrrolidone solvent (NMP, 99%), and electrolytes (1.0 M lithium hexafluorophosphate solution ($LiPF_6$) in ethylene carbonate and dimethyl carbonate (EC/DMC = 50/50 (v/v), battery grade) were purchased from Sigma Aldrich. $FeCl_3$ (98%) and ethanol (98%) were purchased from Fisher. Carbon black (BLACK PEARLS® 2000) was supplied by Cabot.

PPy : CMC binder was synthesized using the same procedure from our previous study.[16] Briefly, we first dissolved 0.4 g Na-CMC (M_W = 250 000 Da) in 80 mL of DI water by magnetic stirring. Next, pyrrole was introduced dropwise into the solution. The mass ratio between pyrrole and CMC is 1 : 1. The beaker containing the mixture was subsequently cooled in an ice bath. After the solution cooled down, the solution of $FeCl_3$, acting as an oxidizing agent, dissolved in 20 mL of DI water was added dropwise into the mixture while stirring vigorously for homogeneous mixing (n_{Pyrole} : n_{FeCl_3} = 1 : 2.75). After 4 h of mixing inside the ice bath, the reaction was then terminated by introducing ethanol into the suspension with 1 : 4 volume ratio of suspension : ethanol. The PPy : CMC precipitate was vacuum filtered, washed several times with ethanol until the filtrate became colorless, and dried at 80 °C for overnight before ground into powder and stored in a desiccator for future use. To prepare Graphite : PPy : CMC electrode slurries, a typical dispersion consisting of 90 wt% graphite and 10 wt% PPy : CMC composite as conductive binder were ball-milled in DI water (the solid content was 20 wt%) for 1 h at 300 rpm in a planetary ball-mill with agate jars and balls. For Graphite : PVDF : C slurries, Graphite, PVDF binder, and conductive additive carbon black (90 : 5 : 5 wt%) were ball-milled in NMP for 4 h, 300 rpm. For Graphite : CMC : C slurries, Graphite, CMC, and carbon black (90 : 5 : 5 wt%) were ball-milled in DI water for 1 h at 300 rpm. The slurries were then cast onto copper film (MTI, battery grade, 9 μm) at a thickness of 10 μm using a doctor blade. The cast films of Graphite : PPy : CMC and Graphite : CMC : C were air-dried at room temperature for 1 h before being punched into electrodes discs with a diameter of 12.7 mm. The cast films of Graphite : PVDF : C on the other hand were dried at 110 °C to remove the NMP solvent before being punched into electrodes discs. All the electrodes (2.0 – 3.0 mg mass loading, density 0.79 ± 0.17 g cm^{-3}) were then dried again at 80 °C under vacuum overnight and brought directly into a glovebox for cell assembly.

Characterization

Scanning electron microscopy (SEM) and energy-dispersive X-ray analysis (EDX) were carried out using a FEI Quanta 650 FEG Environmental SEM, at an accelerating voltage between 10–15 kV. X-ray photoelectron spectroscopy (XPS) measurements were carried out on a Kratos Axis Ultra X-ray Photoelectron Spectrometer. XPS spectra were analyzed using CasaXPS software. Raman spectroscopy was performed using a Raman fiber-optical spectrometer (Wasatch, WP-785-ER-IC, 785 nm). All post-mortem anodes were washed several times with propylene carbonate (PC) inside an Ar-filled glovebox and dried in a vacuum chamber overnight before analysis.

For electrochemical characterization, two-electrode-coin cells (type 2032) were assembled in an argon-filled glovebox (O_2 and H_2O concentrations are maintained at <0.1 ppm). A typical coin cell includes a lithium foil used as both counter and reference electrodes and a graphite composite electrode as the working electrode. The electrolyte (100 μL) was 1 M $LiPF_6$ in EC/DMC (50 : 50 v/v%, Sigma Aldrich). A glass microfiber disc (Whatman®, Grade 934-AH®, pore size: 1.5 μm, thickness: 435 μm, Sigma Aldrich) was used as a separator. Also, a spacer (stainless-steel disc, diameter: 15.5 mm, thickness: 0.5 mm) and a spring (diameter: 15.4 mm, thickness: 0.2 mm),

purchased from MTI, were used. After three formation cycles at 0.1C, the cells were cycled at the same rate for 100 cycles with a BTS battery testing system at room temperature over a voltage of 2–0.01 V. C-rate performance tests were also conducted using the same battery cycler. Cyclic Voltammetry (CV) at 0.1 mV s^{-1} and Electrochemical Impedance Spectroscopy (EIS) with a frequency ranging from 1 MHz to 10 mHz, were performed using a Gamry Interface 1010E potentiostat. All potentials (V) are referenced to the Li/Li^+ (lithium metal) electrode. All electrochemical tests were performed at 24 ± 1 °C. Reported uncertainties represent 95% confidence intervals calculated from replicate measurements ($\geq$3) assuming a Student's *t* distribution.

Results and discussion

The cycling performance of Graphite : PVDF : C, Graphite : CMC : C, and Graphite : PPy : CMC anodes was evaluated over a voltage window of 2–0.01 V *vs.* Li/Li^+, in the presence of industry-standard electrolyte additives (2% v/v vinylene carbonate (VC, Sigma) + 1% v/v 1,3,2-dioxathiolane 2,2-dioxide (DTD, Sigma)). In these compositions, polypyrrole is expected to replace carbon as conductive component. The specific capacity and irreversibility at the 1st SEI formation cycle (0.1C) were calculated to investigate whether PPy : CMC was electrochemically active and participating in any reduction reactions.

As can be seen in Fig. S1, Graphite : PPy : CMC electrodes have the same first lithiation capacity and initial coulombic efficiency within the error (567.1 ± 29.4 mAh g^{-1}, CE = 57.0 ± 2.9%) as compared to Graphite : PVDF : C (570.8 ± 25.7 mAh g^{-1}, CE = 59.6 ± 0.5%) and Graphite : CMC : C (572.4 ± 28.5 mAh g^{-1}, CE = 64.4 ± 3.4%), demonstrating that, unlike other aromatic polymeric binders,[14,15] PPy : CMC was not substantially reduced to carbonaceous conductors during the 1st (de)lithiation. Furthermore, at the same 1st SEI formation cycle, Graphite : PPy : CMC exhibited apparently lower initial delithiation specific capacities of 332.65 ± 12.3 mAh g^{-1}, as compared to Graphite : PVDF : C (339.0 ± 14.7 mAh g^{-1}) and Graphite : CMC : C (345.3 ± 6.8 mAh g^{-1}), though without statistical significance at the 95% confidence level. The large irreversible capacity observed in the first SEI formation cycle is attributed to SEI formation.[17] In the subsequent cycles, both (dis)charge capacities became reversible and approached the practical capacity of graphite (320–360 mAh g^{-1} at low rate of 0.1C), demonstrating good electrochemical performance in the custom cell configurations. After 3 SEI formation cycles, the cells began to cycle at 0.5C for 100 cycles (Fig. 1). The result showed that Graphite : CMC : C still delivered the highest initial delithiation specific capacity of 339.6 ± 24.1 mAh g^{-1}, followed by Graphite : PVDF : C (315.2 ± 20.1 mAh g^{-1}) and Graphite : PPy : CMC (309 ± 31.5 mAh g^{-1}). After 100 cycles at 0.5C, there seems to be little difference in capacity retention between Graphite : PVDF : C and Graphite : CMC : C (~93–94%), whereas Graphite : PPy : CMC exhibited slightly lower capacity retention (~90%). This result shows that Graphite : PPy : CMC can be used in Graphite anode as a conducting binder without the addition of any conducting agent.

Cyclic voltammetry was applied to investigate the impact of the binders on electrode redox behavior. In the 1st cathodic scan (Fig. 2a), a broad reduction peak (centered at around 0.4 V) was observed for all cells. This signal did not appear in subsequent cycles, indicating the irreversible SEI formation

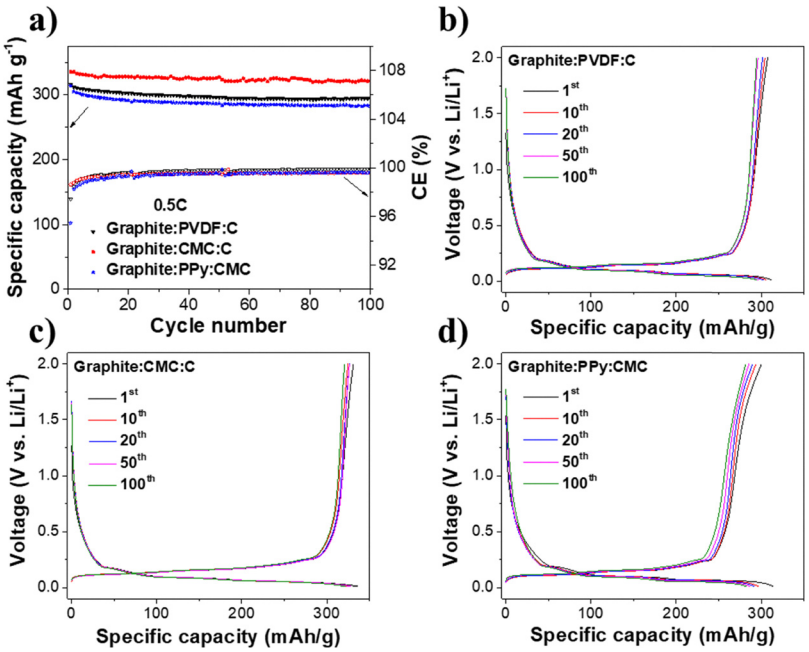

Fig. 1 (a) Cycling performance of Graphite : PVDF : C, Graphite : CMC : C, and Graphite : PPy : CMC half-cells; charge–discharge curves of (b) Graphite : PVDF : C, (c) Graphite : CMC : C, and (d) Graphite : PPy : CMC at 0.5C for 100 cycles (after the first 3 SEI-formation cycles at 0.1C).

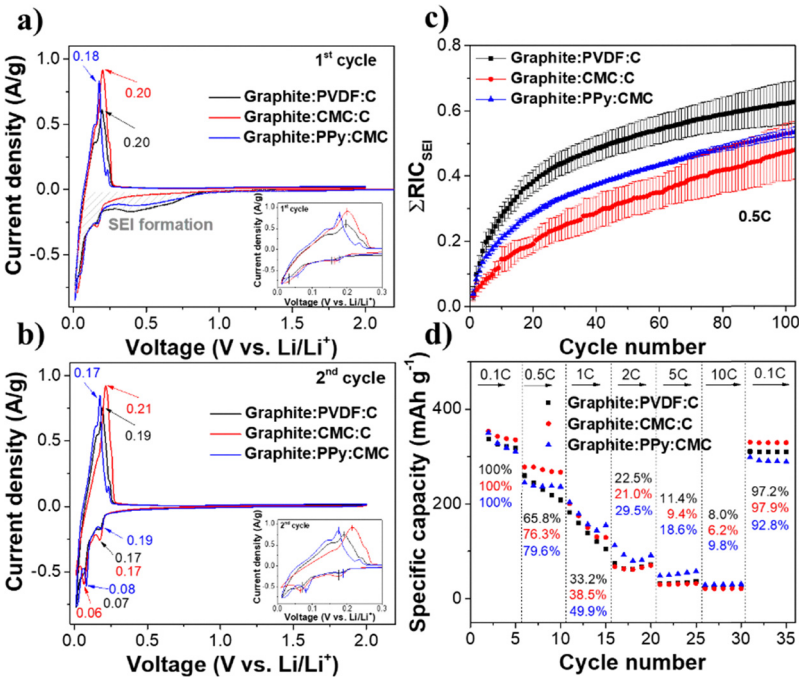

Fig. 2 (a) and (b) Cyclic voltammogram at the 1st and 2nd cycles at 0.1 mV s^{-1}, (c) Cumulative irreversible capacities resulting from SEI formation (ΣRIC_{SEI}) at 0.5C over 100 cycles, and (d) C-rate performance of Graphite : PVDF : C, Graphite : CMC : C, and Graphite : PPy : CMC half-cells.

process. In addition to the SEI-related peaks, subsequent peaks and shoulders resulting from the staged lithiation/delithiation reactions in graphite were reversibly observed in all following cycles (see Fig. S2). Graphite : PPy : CMC showed sharper lithium (de-)intercalation peaks and lower overpotentials (Fig. 2b) compared to Graphite : PVDF : C and Graphite : CMC : C electrodes, suggesting reduced overall resistance and improved charge-transfer kinetics.[18]

A comparison of cumulative irreversible capacities associated with SEI formation (RIC_{SEI}) can be made by calculating the difference between lithiation capacity at cycle n + 1, $Q_{n+1}^{liiation}$ and delithiation capacity of the previous cycle, $Q_n^{deliiation}$, relative to the delithiation capacity at cycle n according to the following equation:

$$\sum \mathrm{RIC_{SEI}} = \sum_{n=1}^{N} \frac{Q_{n+1}^{\mathrm{lithiation}} - Q_n^{\mathrm{delithiation}}}{Q_n^{\mathrm{delithiation}}}$$

Any lithiation in excess of the previous delithiation capacity can be ascribed to electrolyte decomposition, especially when the delithiation capacity is itself degrading. Therefore, ΣRIC_{SEI} reflects accumulated irreversibility, providing an estimate of lithium inventory loss. It can be seen in Fig. 2c that, at 0.5C rate, Graphite : PPy : CMC exhibited lower irreversible capacity than Graphite : PVDF : C and higher than Graphite : CMC : C. The formation of more stable SEI with CMC, through the binder's reactivity with the electrolyte, forming an artificial SEI, has been shown before.[19] The slower SEI formation in Graphite : PPy : CMC and Graphite : CMC : C could also be due to the more homogenous distribution of CMC over the surface of graphite due to the amphiphilic nature of the PPy : CMC and CMC binders, protecting the active material underneath and reducing electrolyte reactivity with the electrode.[20] Finally, prior research clearly demonstrates that the active material - electrolyte contact area has a significant impact on SEI formation. In that context, it should be noted that the replacement of carbon by polypyrrole can cause changes to the conductive surface area of the electrode, where SEI formation can occur. As such, the observed reduced SEI formation may be a result of lower reactivity of the composite electrode due to artificial SEI formation, surface coverage of active electrode components by non-conductive CMC, or lower conductive surface area, due to the larger particle size of PPy (about 50 nm) compared to carbon (primary particle size of 15 nm[21]).

To understand the effect of the binder on the rate performance of graphite anodes, C-rate tests were performed. Fig. 2d shows the C-rate performance of graphite electrodes dependent on the binder system. Both electrodes exhibit typically poor C-rate performance as graphite is an intercalation material with slow intercalation kinetics. Interestingly, as discharge rates increased, the capacity retention of Graphite : PPy : CMC increases slightly compared to Graphite : PVDF : C and Graphite : CMC : C. This can be due to the uniform charge transportation provided by PPy : CMC. Unlike the non-conducting PVDF binder or ion-conducting CMC binder, where electron transfer happens only at the points contacting the active material with carbon particles, the balanced dual functionality of PPy : CMC, *i.e.*, electronic conductivity from PPy and ionic conductivity from CMC, provides the continuous transport of ions and electrons over the surface of the active material. This contributes to better electrical contact and charge distribution,

ultimately leading to better performance at high C-rates, where charge transfer of both electrons and ions is challenged.[22]

More insight into the kinetic properties of graphite electrodes was obtained from EIS data. Fig. 3a–c show the Nyquist plots of the batteries after resting for 10 hours, SEI formation, and 10th, 20th, 50th, and 100th cycles. Initially, only one charge transfer process (semicircle) was observed for all cells. As the number of cycles increased, the SEI thickened, resulting in the appearance of a second charge transfer process in the high-frequency range. Generally, the higher frequency process is ascribed to interfacial layer resistance, which is related to the impedance of Li-ion migration through the SEI, R_{SEI}.[23] The main charge transfer process, observed in the intermediate-frequency range, represents the charge transfer between the electrode and the electrolyte, R_{ct}. The diffusion-dependent Warburg impedance (W_o), represented by a straight 45° slope, is observed at low frequency (see Fig. S3). Using the equivalent circuit $R_s + CPE_{SEI}/R_{SEI} + CPE_{ct}/(R_{ct} + W)$, where CPE is constant phase element (Fig. 3, inset), the charge transfer resistance R_{ct} was calculated (Fig. 3d).

If the reduction of PPy : CMC during cycling caused significant electronic resistance growth in the composite electrode, an increase in the R_{ct} or R_s values would be expected. However, no reproducible increase was found in Graphite : PPy : CMC, consistent with the behavior of Graphite : PVDF : C and Graphite : CMC : C (Fig. S3d). While this is not direct evidence of a lack of PPy reduction, it indicates minimal impact on the electrode resistance. The charge transfer resistance R_{ct} of all the samples showed a similar decrease over cycling. Interestingly, throughout cycling, Graphite : PVDF : C and Graphite : PPy : CMC exhibited lower R_{ct} than Graphite : CMC : C (Fig. 3d), potentially indicating better connectivity within those binder systems.

Scanning electron microscopy with energy dispersive X-ray spectroscopy (SEM/EDX) was conducted to examine the morphology and possible compositional changes due to the SEI formation at electrode surfaces. As shown in Fig. S4 (left side), the pristine electrodes showed homogeneous particle distribution for both types of electrodes. No obvious morphological changes were observed after cycling. From the EDX results (Fig. S4 (right side)), the presence of nitrogen from PPy rings ($4.8 \pm 0.6\%$) and fluorine from PVDF ($1.9 \pm 0.2\%$) was detected on the surface of the pristine Graphite : PPy : CMC and Graphite : PVDF : C electrodes, respectively. After cycling, both electrodes exhibited signs of SEI formation through an increase in oxygen, fluorine, and phosphorus atomic fractions.

The elemental composition at the electrode surface was analyzed using X-ray photoelectron spectroscopy (XPS). The C 1s spectra (Fig. S5) of three pristine electrodes show the main peak at 284.8–285.0 eV corresponding to the sp^2-hybridized carbon C–C of the graphite active material.[24] The spectra of Graphite : PVDF : C indicate the presence of the covalent C–F (C 1s at 288.3 eV and F 1s at 687.9 eV) and C–F_2 (C 1s at 291.0 eV and F 1s at 688.8 eV) bonds from PVDF binder,[18] which are absent in Graphite : PPy : CMC and Graphite : CMC : C, as well as the carbon atoms single-bonded to hydrogen (C–H, C 1s at 285.0 eV).[24] The spectra of Graphite : PPy : CMC reveal the features of C–N bonds from the pyrrole ring (C 1s at 285.0 eV, N 1s at 399.8 eV), and C–O (C 1s at 286.4 eV, O 1s at 533.5 eV) and C═O bonds (C 1s at 291.0 eV, O 1s at 532.0 eV) from the CMC component.[25] The characteristic peak of PPy : CMC (C–N,

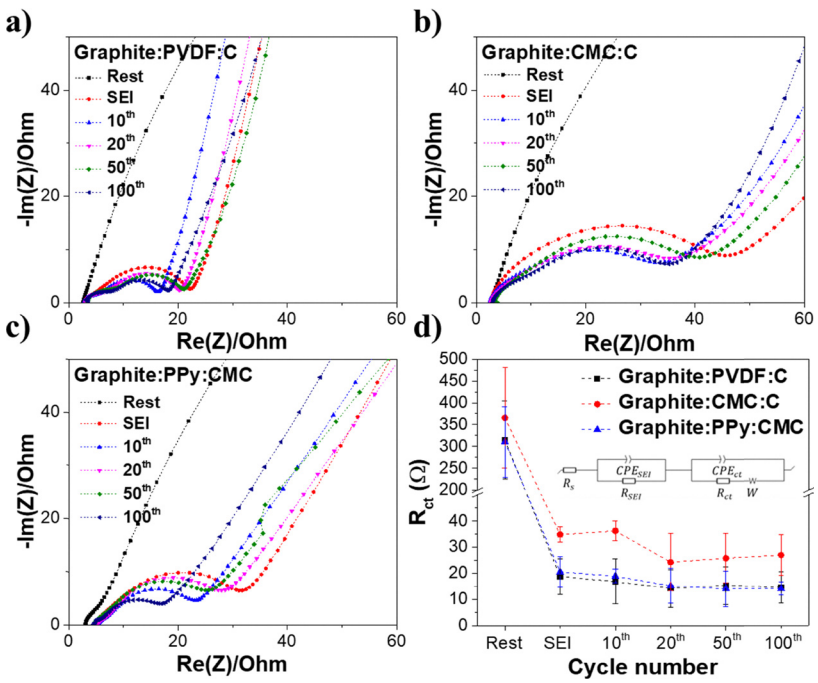

Fig. 3 Representative Nyquist plots of (a) Graphite : PVDF : C, (b) Graphite : CMC : C, (c) Graphite : PPy : CMC cells; and (d) calculated charge transfer resistance R_{ct} (Ω) after resting, SEI formation, 10th, 20th, 50th, and 100th cycles, in delithiated state, and the equivalent circuit model (inset) for fitting the EIS data.

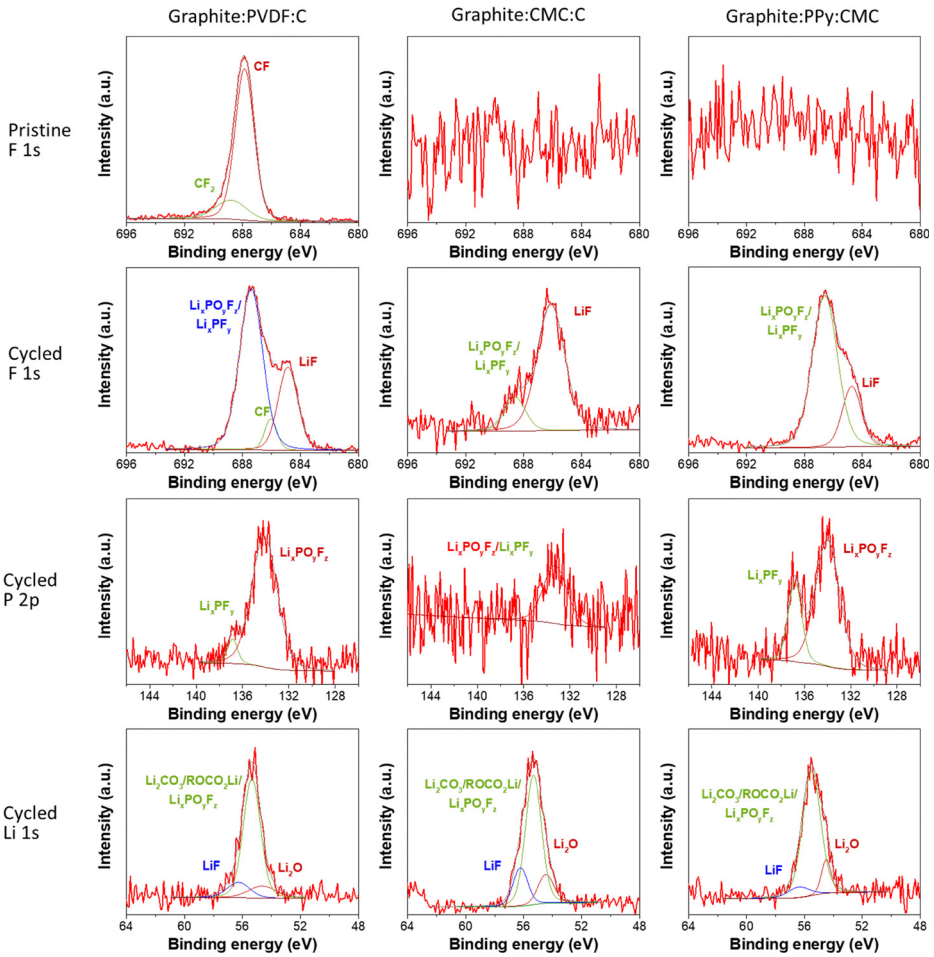

Fig. 4 XPS spectra of F 1s, P 2p, and Li 1s of Graphite : PVDF : C, Graphite : CMC : C, and Graphite : PPy : CMC electrodes before and after 100 cycles at 0.5C.

399.8 eV) decreased after 100 cycles (Fig. S6a and b). As XPS is highly surface-sensitive, this is likely a result of SEI formation and coverage of any conductive binder surfaces. For Graphite : CMC : C, XPS shows several peaks from CMC, such as C–O/C–OH (C 1s at 286.8 eV, O 1s at 533.8 eV), C═O (C 1s at 290.2 eV, O 1s at 533.2 eV), and C–O–C (O 1s at 536.2 eV) (Table S1).

SEI chemistry was also reflected in XPS spectra. Fig. 4 shows the spectra of F 1s, P 2p, and Li 1s, which provides insight into SEI components of the electrodes. The SEI surface of Graphite : PVDF : C mainly contains Li_2CO_3 (C 1s at 290.4 eV, O 1s at 532.1 eV, and Li 1s at 55.4 eV), lithium alkoxides/lithium alkyl carbonates ($ROLi/ROCO_2Li$) (C 1s at 289.1 eV, O 1s 531.4 eV and Li 1s at 55.4 eV), $Li_xPO_yF_z$ (O 1s at 533.8 eV, F 1s at 687.4eV, P 2p at 134.1 eV, and Li 1s at 55.4 eV), LiF (F 1s at 684.8 eV and Li 1s at 56.3 eV), as well as Li_2O (Li 1s at 54.6 eV).[24,26–28] Similar compounds were found in the spectra of cycled Graphite : PPy : CMC electrodes (see Table S1). The C 1s and O 1s spectra show significant growth of components at higher binding energies after cycling, suggesting oxidative decomposition of the electrolyte solvent occurred on all electrodes, producing organic species. The F 1s spectra indicate the presence of electrolyte decomposition by-products, such as LiF, Li_xPF_y, and $Li_xPO_yF_z$. The atomic percentages of F, P, and Li, calculated from survey spectra (Fig. S6c), showed that Graphite : PPy : CMC exhibits SEI chemistry similar to Graphite : PVDF : C and Graphite : CMC : C.

To study the potential reduction of PPy : CMC in the electrode, Raman measurements were carried out. As can be seen in Fig. 5, graphite's characteristic peaks were observed at 1314 cm^{-1} (D-band) and 1580 cm^{-1} (G-band)[29] in the Raman spectra of all samples before and after cycling. For Graphite : PPy : CMC, signals of PPy were detected in both the pristine and cycled electrodes. The presence of oxidized PPy was identified by the peak at 928 cm^{-1}, ascribed to the ring deformation related to the bipolaron structure of PPy, and the peak at 1605 cm^{-1} attributed to the stretching of C═C backbone in the oxidized PPy.[30,31] After 100 cycles, the PPy signal at 928 cm^{-1} weakened significantly, and a new peak at 987 cm^{-1} appeared, indicating the reduction of PPy.[31,32] These results suggest that PPy : CMC was partially reduced, accompanied by the loss of the bipolaron structure. Such reduction is accompanied by diminished electronic conductivity. While EIS and cycling performance data show little impact of such reduction, electrodes with higher mass loading may experience greater sensitivity to the binder domain conductivity. The binder's function as a binding agent

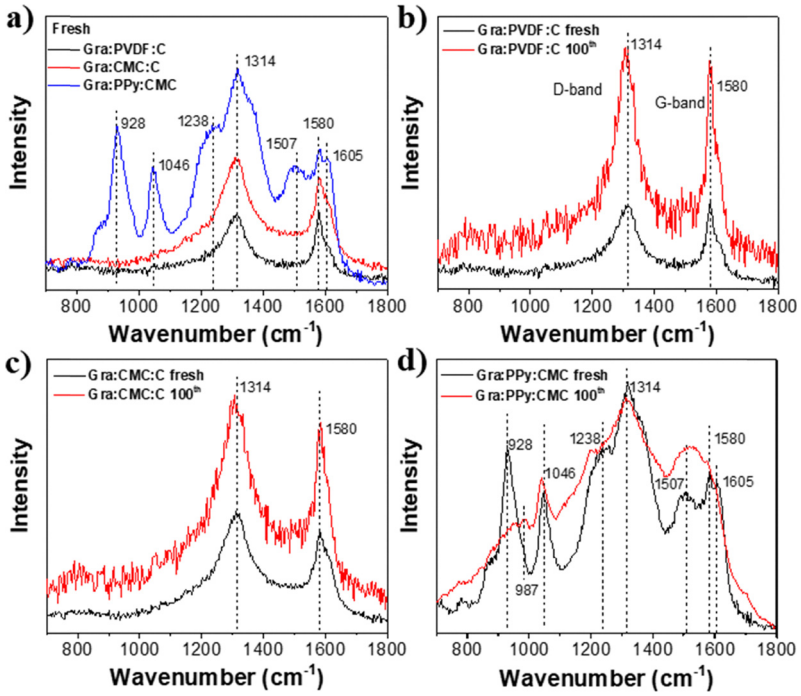

Fig. 5 Raman spectra of (a) fresh electrodes; (b) Graphite : PVDF : C, (c) Graphite : CMC : C, and (d) Graphite : PPy : CMC electrodes, fresh and after 100 cycles at 0.5C.

remains stable during long-term cycling, as evidenced by the long-term cycling profiles of Graphite : PPy : CMC after 1000 cycles at 0.1C and 500 cycles 0.5C (see Fig. S7 and Fig. S8).

Conclusions

Aqueous electrode processing offers the potential to reform conventional binder technology without compromising on electrochemical performance. Our work shows that PPy : CMC as a binder provides several advantages, including cost and energy savings from lower temperature drying, elimination of solvent recovery, and avoidance of PFAS, leading to more ecofriendly electrode manufacturing. When used in graphite electrodes, PPy : CMC can serve as the sole electrode additive, delivering performance comparable to the industry-standard PVDF : C. Considering electrolyte side reactions, it is well known that the poor stability of the SEI film leads to lithium-ion consumption and thus, increasing cumulative irreversible capacities, ΣRIC_{SEI}. According to XPS spectra, the SEI film is composed of an inorganic layer of Li_2CO_3, Li_2O, LiF, $Li_xPO_yF_z$, and organic lithium salts such as $ROCO_2Li$ and ROLi. ΣRIC_{SEI} findings suggest that SEI layer formation seems to happen slower when using PPy : CMC. In addition, the presence of the oxidized PPy peaks in Raman spectra before cycling and reduced PPy after cycling indicates partial reduction of PPy : CMC during cycling. Despite the partial reduction, PPy : CMC maintains stable binding, as shown by long-term cycling. However, an in-depth understanding of the impact of PPy reduction in other lithium-intercalation anode compositions and the binder behavior in full-cell configuration remain to be established. This research paves the way for further development of aqueous and conducting binders to eliminate the need for toxic solvents and move a step closer to sustainable and eco-friendly production to meet the continuously growing demand for LIBs.

Author contributions

Anh Ngoc Tram Mai: methodology, investigation, data analysis, writing – original draft preparation and editing. Christian Kuss: supervising, writing – reviewing and editing.

Conflicts of interest

There are no conflicts to declare.

Data availability

All data generated or analyzed during this study are included in this published article and its supplementary information (SI). Supplementary information: SEI formation cycles, CV cycles 1–5, 1st cycle EIS Nyquist plot, solution resistance (R_s), SEM images, XPS spectra and data, long-term cycling to 500/1000 cycles. See DOI: https://doi.org/10.1039/d6ya00042h.

Acknowledgements

The research was funded by the Natural Sciences and Engineering Research Council of Canada (NSERC) through the Discovery

Grant Program, and the University of Manitoba. We thank Ravinder Sidhu from Manitoba Institute for Materials (MIM) for performing the XPS characterization.

References

1 K. E. Aifantis, S. A. Hackney and R. V. Kumar *High energy density lithium batteries*, Wiley Online Library, 2010.
2 W. Dou, M. Zheng, W. Zhang, T. Liu, F. Wang, G. Wan, Y. Liu and X. Tao, Review on the Binders for Sustainable High-Energy-Density Lithium Ion Batteries: Status, Solutions, and Prospects, *Adv. Funct. Mater.*, 2023, **33**(45), 202305161, DOI: 10.1002/adfm.202305161.
3 Q. He, J. Ning, H. Chen, Z. Jiang, J. Wang, D. Chen, C. Zhao, Z. Liu, I. F. Perepichka, H. Meng and W. Huang, Achievements, challenges, and perspectives in the design of polymer binders for advanced lithium-ion batteries, *Chem. Soc. Rev.*, 2024, **53**(13), 7091–7157, DOI: 10.1039/D4CS00366G.
4 F. Zou and A. Manthiram, A Review of the Design of Advanced Binders for High-Performance Batteries, *Adv. Energy Mater.*, 2020, **10**(45), 2002508, DOI: 10.1002/aenm.202002508.
5 A. Samridh, S. V. Gopinadh, B. John, S. Sarojiniamma, M. T. Devassia and M. G. Joseph, Sustainable Binder System: Cross-Linked Tamarind Gum-Polyacrylic Acid for Silicon-Graphite Anodes in Future Lithium-Ion Batteries, *Energy Technol.*, 2025, **13**(5), 2401837, DOI: 10.1002/ente.202401837.
6 N. Lingappan, L. Kong and M. Pecht, The significance of aqueous binders in lithium-ion batteries, *Renewable Sustainable Energy Rev.*, 2021, **147**, 111227, DOI: 10.1016/j.rser.2021.111227.
7 A. M. Pillai, P. S. Salini, B. John and M. T. Devassy, Aqueous Binders for Cathodes: A Lodestar for Greener Lithium Ion Cells, *Energy Fuels*, 2022, **36**, 5063–5087, DOI: 10.1021/acs.energyfuels.2c00346.
8 Y. Wang, Q. Wen, Y. Chen and W. Li, Conductive polypyrrole-carboxymethyl cellulose-titanium nitride/carbon brush hydrogels as bioanodes for enhanced energy output in microbial fuel cells, *Energy*, 2020, **204**, 117942, DOI: 10.1016/j.energy.2020.117942.
9 V. A. Nguyen, J. Wang and C. Kuss, Conducting polymer composites as water-dispersible electrode matrices for Li-Ion batteries: Synthesis and characterization, *J. Power Sources Adv.*, 2020, **6**, 100033, DOI: 10.1016/j.powera.2020.100033.
10 Y. Xu and Y. Zhang, Synthesis of polypyrrole/sodium carboxymethyl cellulose nanospheres with enhanced supercapacitor performance, *Mater. Lett.*, 2015, **139**, 145–148, DOI: 10.1016/j.matlet.2014.10.074.
11 Y. Wang, X. Pan, Y. Chen, Q. Wen, C. Lin, J. Zheng, W. Li, H. Xu and L. Qi, A 3D porous nitrogen-doped carbon nanotube sponge anode modified with polypyrrole and carboxymethyl cellulose for high-performance microbial fuel cells, *J. Appl. Electrochem.*, 2020, **50**(12), 1281–1290, DOI: 10.1007/s10800-020-01488-z.
12 M. Tanzifi, M. T. Yaraki, Z. Beiramzadeh, L. H. Saremi, M. Najafifard, H. Moradi, M. Mansouri, M. Karami and H. Bazgir, Carboxymethyl cellulose improved adsorption capacity of polypyrrole/CMC composite nanoparticles for removal of reactive dyes: Experimental optimization and DFT calculation, *Chemosphere*, 2020, **255**, 127052, DOI: 10.1016/j.chemosphere.2020.127052.
13 C. Sasso, D. Beneventi, E. Zeno, D. Chaussy, M. Petit-Conil and N. Belgacem, Polypyrrole and polypyrrole/wood-derived materials conducting composites: a review, *BioResources*, 2011, **6**(3), 3585–3620.
14 T. D. Hatchard, P. Bissonnette and M. N. Obrovac, Phenolic Resin as an Inexpensive High Performance Binder for Li-Ion Battery Alloy Negative Electrodes, *J. Electrochem. Soc.*, 2016, **163**, A2035–A2039, DOI: 10.1149/2.1121609jes.
15 B. N. Wilkes, Z. L. Brown, L. J. Krause, M. Triemert and M. N. Obrovac, The Electrochemical Behavior of Polyimide Binders in Li and Na Cells, *J. Electrochem. Soc.*, 2015, **163**, A364–A372, DOI: 10.1149/2.0061603jes.
16 V. A. Nguyen, J. Wang and C. Kuss, Conducting polymer composites as water-dispersible electrode matrices for Li-Ion batteries: Synthesis and characterization, *J. Power Sources Adv.*, 2020, **6**, 100033, DOI: 10.1016/j.powera.2020.100033.
17 E. M. C. Jones, Ö. Ö. Çapraz, S. R. White and N. R. Sottos, Reversible and Irreversible Deformation Mechanisms of Composite Graphite Electrodes in Lithium-Ion Batteries, *J. Electrochem. Soc.*, 2016, **163**, A1965–A1974, DOI: 10.1149/2.0751609jes.
18 Z.-X. Zhao, X. Bai, H. L. Zhu, W. Liu, Y. X. Qi, T. Li and Y. J. Bai, Promoting the Normal- and Low-Temperature Performances of Natural Graphite by the F-Doping Derived from PVDF Modification, *ACS Appl. Electron. Mater.*, 2022, **4**(10), 4936–4946, DOI: 10.1021/acsaelm.2c00939.
19 D. Bresser, D. Buchholz, A. Moretti, A. Varzi and S. Passerini, Alternative binders for sustainable electrochemical energy storage–the transition to aqueous electrode processing and bio-derived polymers, *Energy Environ. Sci.*, 2018, **11**, 3096–3127, DOI: 10.1039/C8EE00640G.
20 W. J. Chang, G. H. Lee, Y. J. Cheon, J. T. Kim, S. I. Lee, J. Kim, M. Kim, W. I. Park and Y. J. Lee, Direct Observation of Carboxymethyl Cellulose and Styrene-Butadiene Rubber Binder Distribution in Practical Graphite Anodes for Li-Ion Batteries, *ACS Appl. Mater. Interfaces*, 2019, **11**(44), 41330–41337, DOI: 10.1021/acsami.9b13803.
21 A. Macias-Garcia, M. A. Diaz-Diez, M. Alfaro-Dominguez and J. P. Carrasco-Amador, Influence of chemical composition, porosity and fractal dimension on the electrical conductivity of carbon blacks, *Heliyon*, 2020, **6**, e04024, DOI: 10.1016/j.heliyon.2020.e04024.
22 S. N. Eliseeva, M. A. Kamenskii, E. G. Tolstopyatova and V. V. Kondratiev, Effect of Combined Conductive Polymer Binder on the Electrochemical Performance of Electrode Materials for Lithium-Ion Batteries, *Energies*, 2020, **13**, 2163, DOI: 10.3390/en13092163.
23 Z. Li, J. Liu, Y. Qin and T. Gao, Enhancing the Charging Performance of Lithium-Ion Batteries by Reducing SEI and

Charge Transfer Resistances, *ACS Appl. Mater. Interfaces*, 2022, **14**, 33004–33012, DOI: 10.1021/acsami.2c04319.

24 L. Huang, S. Chen, J. Zhan, J. Liang, S. Li, H. Wang, M. Xu and W. Li, Insight into the Role of Fluoroethylene Carbonate in Solid Electrolyte Interphase Construction for Graphite Anodes of Lithium-Ion Batteries, *J. Phys. Chem. C*, 2024, **128**(23), 9586–9594, DOI: 10.1021/acs.jpcc.4c02475.

25 M. Chen, Z. Yan, J. Luan, X. Sun, W. Liu and X. Ke, π–π electron-donor-acceptor (EDA) interaction enhancing adsorption of tetracycline on 3D PPY/CMC aerogels, *Chem. Eng. J.*, 2023, **454**(4), 140300, DOI: 10.1016/j.cej.2022.140300.

26 F. Allgayer, J. Maibach and F. Jeschull, Comparing the Solid Electrolyte Interphases on Graphite Electrodes in K and Li Half Cells, *ACS Appl. Energy Mater.*, 2022, **5**, 1136–1148, DOI: 10.1021/acsaem.1c03491.

27 J. Światowska, V. Lair, C. Pereira-Nabais, G. Cote, P. Marcus and A. Chagnes, XPS, XRD and SEM characterization of a thin ceria layer deposited onto graphite electrode for application in lithium-ion batteries, *Appl. Surf. Sci.*, 2011, **257**(21), 9110–9119, DOI: 10.1016/j.apsusc.2011.05.108.

28 T. Zhu, Q. Hu, G. Yan, J. Wang, Z. Wang, H. Guo, X. Li and W. Peng, Manipulating the Composition and Structure of Solid Electrolyte Interphase at Graphite Anode by Adjusting the Formation Condition, *Energy Technol.*, 2019, **7**(9), 1900273, DOI: 10.1002/ente.201900273.

29 A. Beda, S. Zallouz, S. Hajjar-Garreau, H. El Marouazi, L. Simonin and C. Matei Ghimbeu, Impact of Na-Carboxymethyl Cellulose Binder Type on Hard Carbon Performance and SEI Formation in Sodium-Ion Batteries, *ACS Appl. Mater. Interfaces*, 2024, **16**(49), 68664–68679, DOI: 10.1021/acsami.4c15906.

30 Y. Hou, L. Zhang, L. Y. Chen, P. Liu, A. Hirata and M. W. Chen, Raman characterization of pseudocapacitive behavior of polypyrrole on nanoporous gold, *Phys. Chem. Chem. Phys.*, 2014, **16**(8), 3523–3528, DOI: 10.1039/c3cp54497d.

31 M. J. L. Santos, A. G. Brolo and E. M. Girotto, Study of polaron and bipolaron states in polypyrrole by in situ Raman spectroelectrochemistry, *Electrochim. Acta*, 2007, **52**, 6141–6145, DOI: 10.1016/j.electacta.2007.03.070.

32 H. Nguyen Thi Le, Raman spectroscopy analysis of polypyrrole films as protective coatings on iron, *Synth. Met.*, 2004, **140**, 287–293, DOI: 10.1016/s0379-6779(03)00376-x.